

SUPPORTING INFORMATION

Nanoparticle-Mediated Acoustic Cavitation Enables High Intensity Focused Ultrasound Ablation Without Tissue Heating

Adem Yildirim,^{,†} Dennis Shi,[†] Shambojit Roy,[†] Nicholas T. Blum,[†] Rajarshi Chattaraj,[‡]
Jennifer N. Cha,[†] and Andrew P. Goodwin^{*,†}*

[†]Department of Chemical and Biological Engineering, University of Colorado Boulder. Boulder,
Colorado 80303, United States

[‡]Department of Mechanical Engineering, University of Colorado Boulder. Boulder, Colorado 80309,
United States

HIFU TRANSDUCER CALIBRATION

Pressure measurements. To estimate the peak positive and negative pressures at the focal zone of HIFU pulses (Figure S1 and Table S1), the following strategy was applied:

Waveform measurements were performed using a pulse duration of 14.1 μs (12 cycles) and pulse repetition frequency of 10 Hz.

1) The hydrophone (HGL-0400, Onda) was placed 5 cm away from the focus, and a glass slide was placed in between the hydrophone and the transducer (3 cm away from the focal point of the transducer) to attenuate the acoustic pressures by a factor of 3.6, as determined from an average of 12 measurements. The output signals were measured for a waveform generator output between 100 mV and 1.4 V.

2) Next, a scaling factor was calculated to determine the change in hydrophone measurement between the focal zone and the defocused zone from Step 1. Output signals were collected from a waveform generator output of 90 mV both at the focus and 5 cm away from the focus. Accordingly, a scaling factor of 38-fold was measured for both peak positive and negative pressures.

3) Finally, the focal peak positive and negative pressures were estimated by multiplying the output measured in Step 1 by both the scaling factor calculated in Step 2 and the glass slide attenuation factor from Step 1.

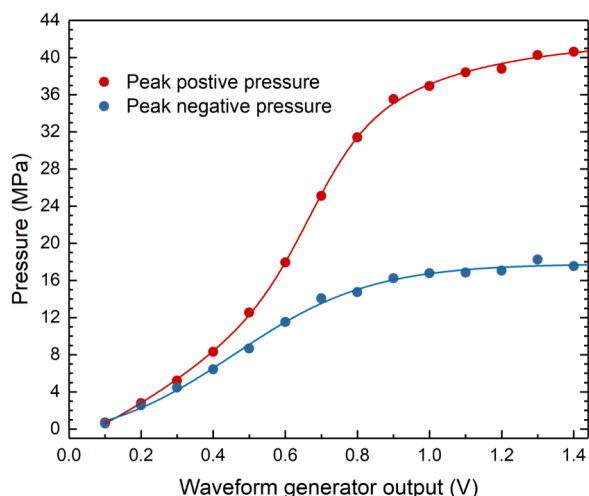


Figure S1. Estimated peak positive and negative pressures of the HIFU pulses at the focal zone as a function of output voltage.

Table S1. The peak positive and negative pressures a function of output voltage used in this study.

Waveform Generator Output, Vpp	Peak Positive Pressure (MPa)	Peak Negative Pressure (MPa)
0.3	5.2	4.5
0.4	8.3	6.4
0.6	17.9	11.5
0.8	31.4	14.7
1	36.9	16.8
1.2	38.8	17.1
1.4	40.6	17.5

Pulse duration measurements. To determine the pulse durations, waveforms were measured at the focus of the HIFU transducer using a waveform generator output of 90 mV and different number of cycles (number of sine waves in a pulse) between 1 and 18. Then, using the waveforms the pressure-squared integral vs time graphs were plotted and pulse duration were calculated using the formula below.¹

$$\text{pulse duration} = 1.25(t_2 - t_1)$$

where t_1 and t_2 are the time points at which pressure-squared integral value reaches 10% and 90% of its maximum value, respectively.

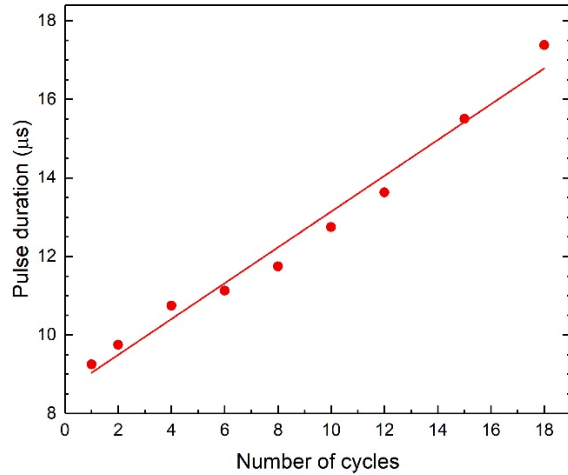


Figure S2. Calculated pulse durations as function of number of cycles in a pulse.

Focal dimension measurements. To determine the focal dimensions, peak negative pressure measurements (at 90 mV waveform generator output, pulse duration of 14.1 μs , and pulse repetition frequency of 10 Hz) were performed by moving the hydrophone in small steps through x and z axes using a micrometer stage. Accordingly, focal length and diameter of the HIFU beam, defined as the width of the -6 dB region, were calculated to be 6 mm and 1.2 mm, respectively.

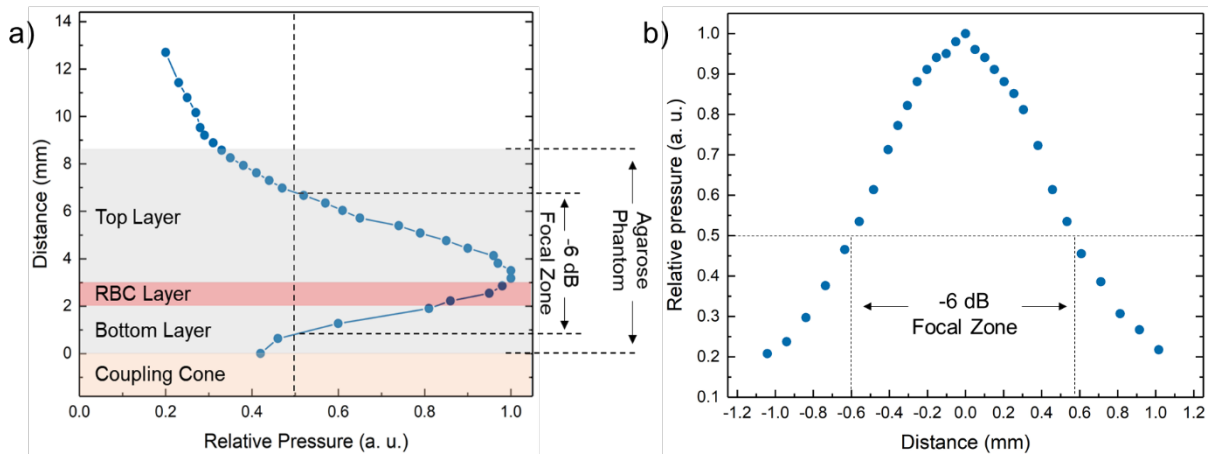


Figure S3. HIFU transducer focal zone measurements. a) Change in relative peak negative pressure through z axis. The dimensions of the agarose phantoms were also added to the graph to show the position of RBC layer in the focal zone. b) Change of the relative peak negative pressure through the x-axis.

SUPPORTING FIGURES

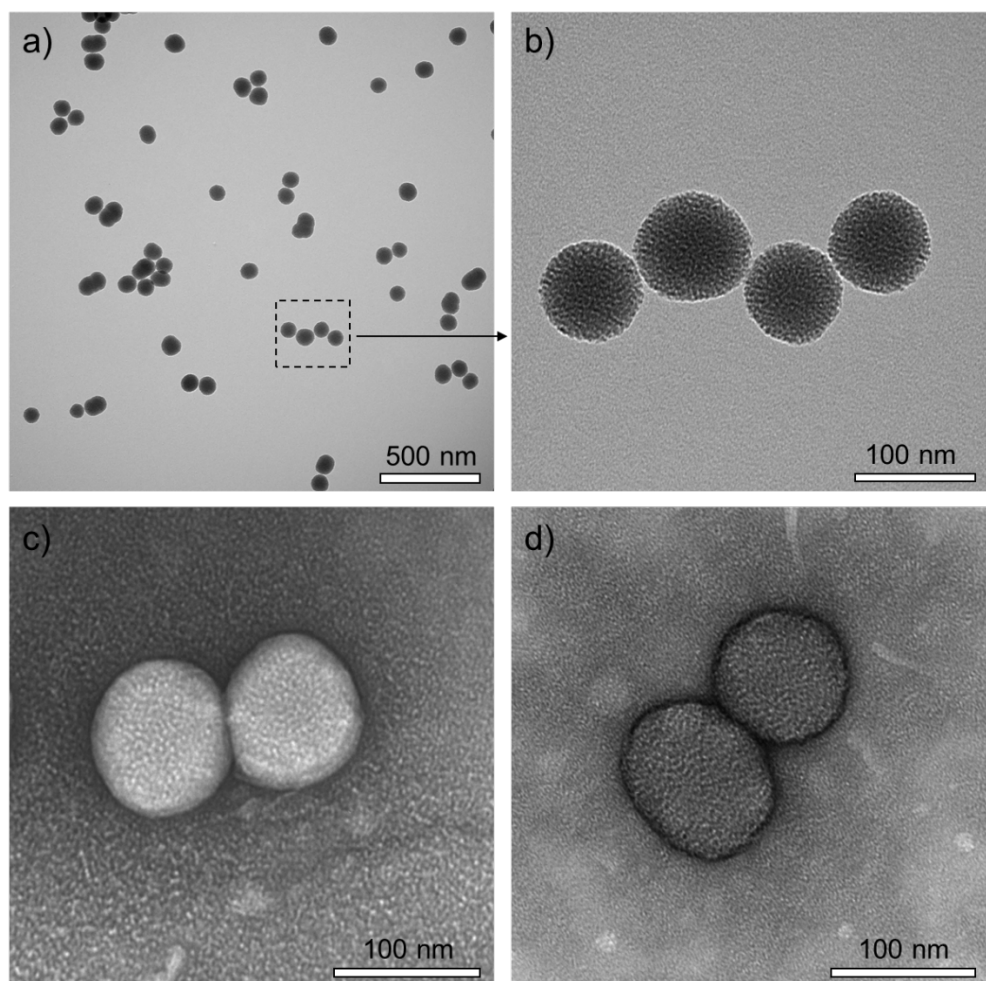


Figure S4. TEM images of the nanoparticles. a) and b) Fluorescein labeled MSNs, c) PL-hMSN stained with uranyl acetate. d) MSN stained with uranyl acetate.

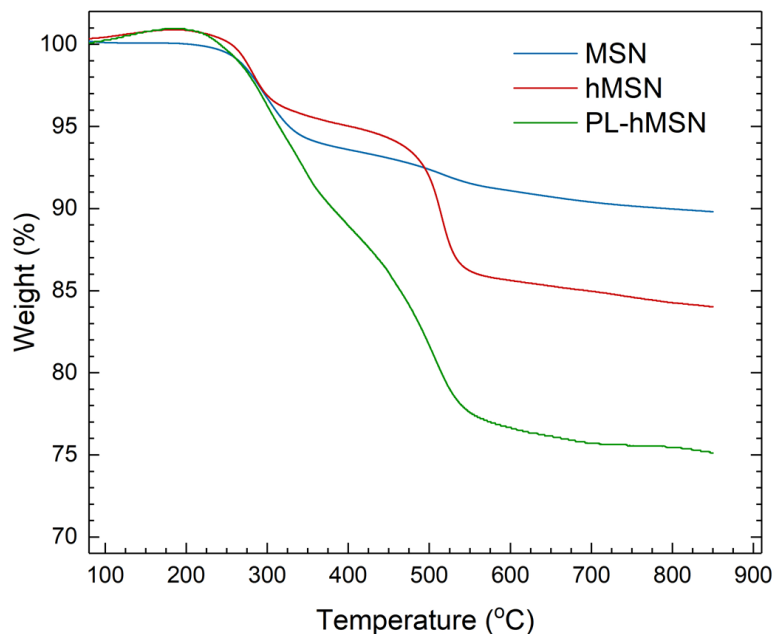


Figure S5. TGA analysis of MSN, hMSN, and PL-hMSN. The weight loss between 150 and 600 °C can be used to estimate the organic content of the particles.² In this region, a weight loss of 9 % was observed for MSN, which was mainly due to the decomposition of the fluorescein and residual surfactant molecules. Also, dehydroxylation of the silica surface at high temperatures can contribute to this weight loss.² For hMSN, the weight loss was higher (15%) due to the removal of dodecyl groups bound to the nanoparticle surface. Finally, weight loss increased by 9 % for PL-hMSN, which can be attributed to the removal of the phospholipid molecules.

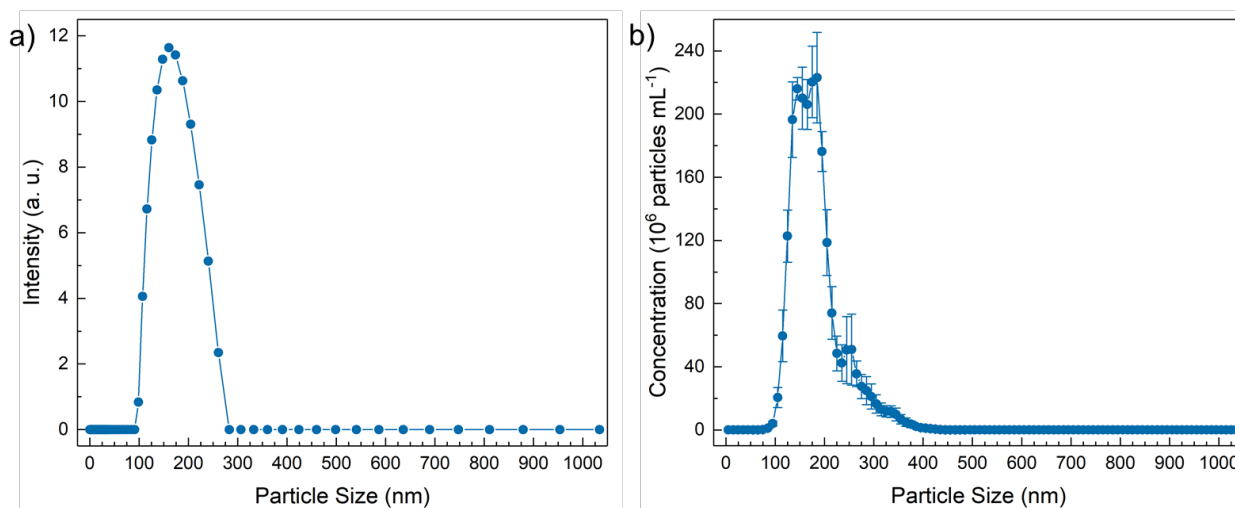


Figure S6. Size distributions of PL-hMSN in PBS (pH 7.4, 10 mM) as determined by a) dynamic light scattering and b) nanoparticle tracking analysis.

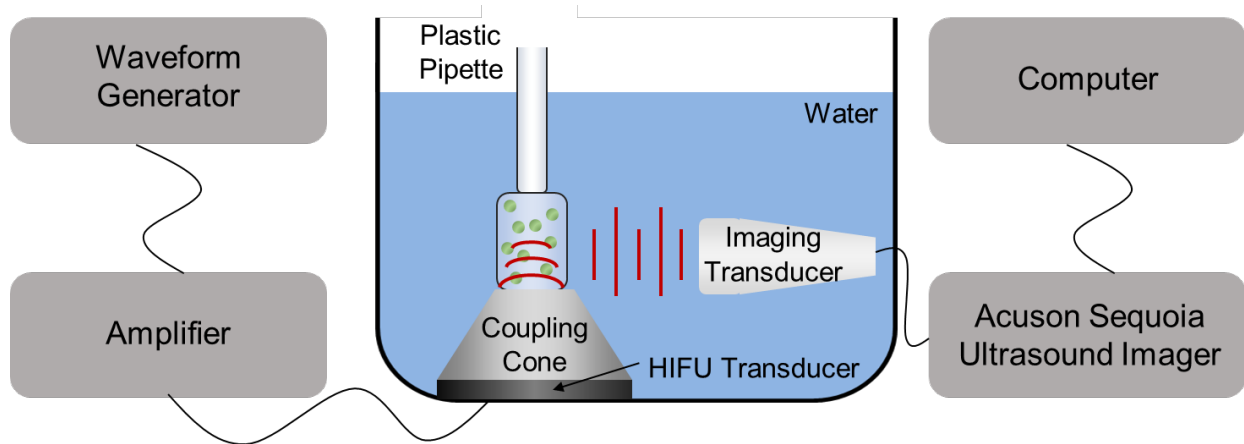


Figure S7. Schematic representation of the experimental set-up used to determine acoustic cavitation generated by the nanoparticles.

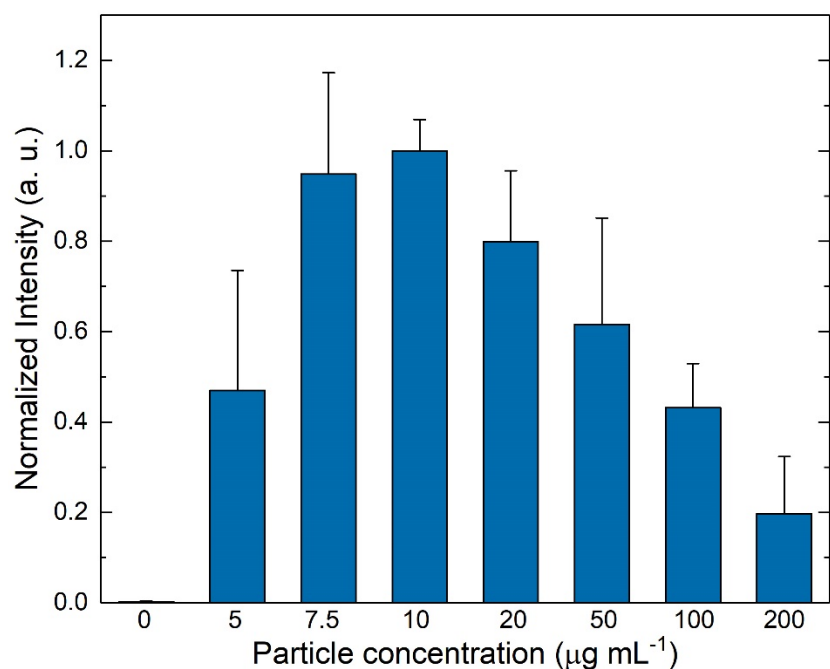


Figure S8. Normalized ultrasound contrast intensities from the acquired movies of PL-hMSN samples dispersed in PBS at different concentrations. Samples were exposed to HIFU for 15 s at a pulse duration of 14.1 μs , a pulse repetition frequency of 10 Hz (duty cycle of 0.014%), and peak negative pressure of 16.8 MPa. The gradual decrease in the ultrasound contrast intensity at concentrations higher than 10 $\mu\text{g mL}^{-1}$ can be due to the increased rate of destruction of the generated bubbles by the increased number of acoustic cavitation events at higher particle concentration.³ Error bars = 1 SD, studies were run in triplicate.

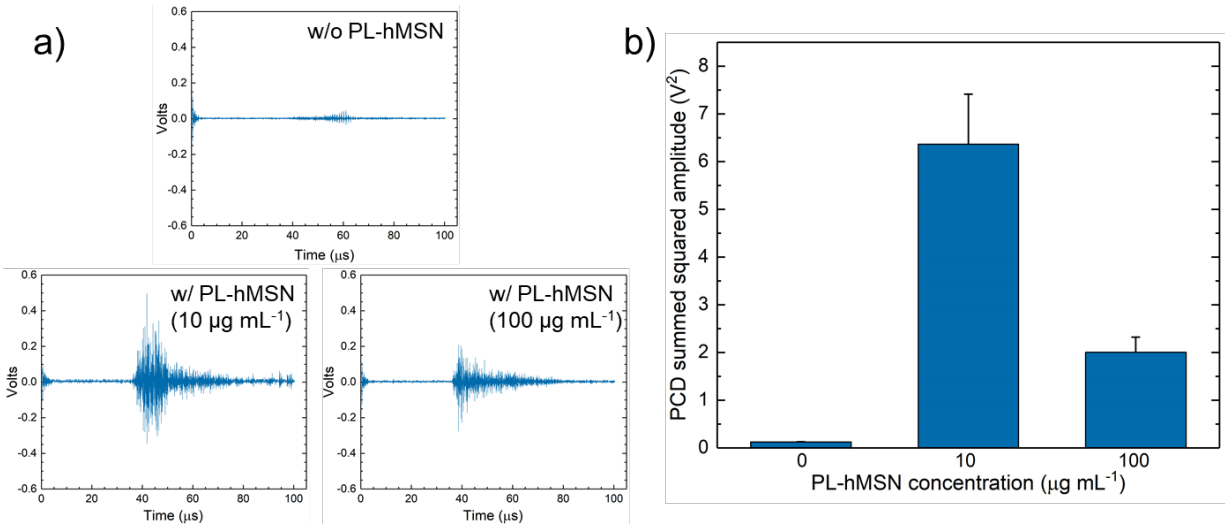


Figure S9. a) Representative oscilloscope readings for PL-hMSN solutions at different concentrations. b) The summed and squared corresponding PCD responses. Samples were exposed to HIFU at a pulse duration of 14.1 μs, a pulse repetition frequency of 10 Hz (duty cycle of 0.014%), and peak negative pressure of 16.8 MPa. Error bars = 1 SD, studies were run in triplicate.

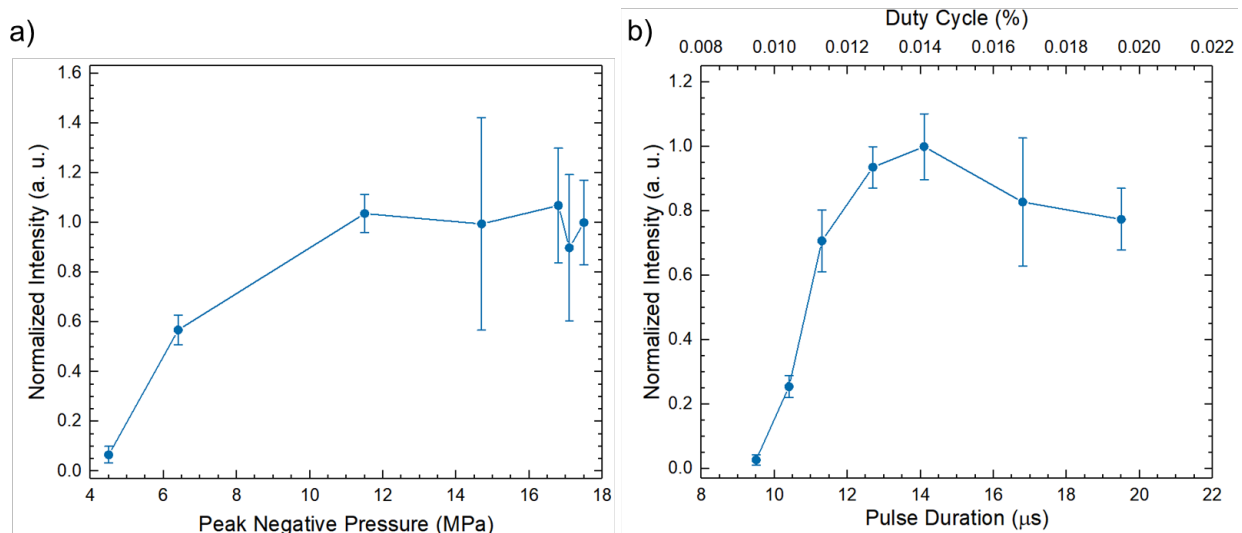


Figure S10. Normalized ultrasound contrast intensities from the acquired movies of PL-hMSN (200 μg mL⁻¹) samples dispersed in 1% agarose gels. a) Samples were exposed to HIFU for 15 s at different peak negative pressures at a pulse duration of 16.8 μs and a pulse repetition frequency of 10 Hz (duty cycle of 0.017%). b) Samples were exposed to HIFU for 15 s at different pulse durations at a pulse repetition frequency of 10 Hz and peak negative pressure of 16.8 MPa.

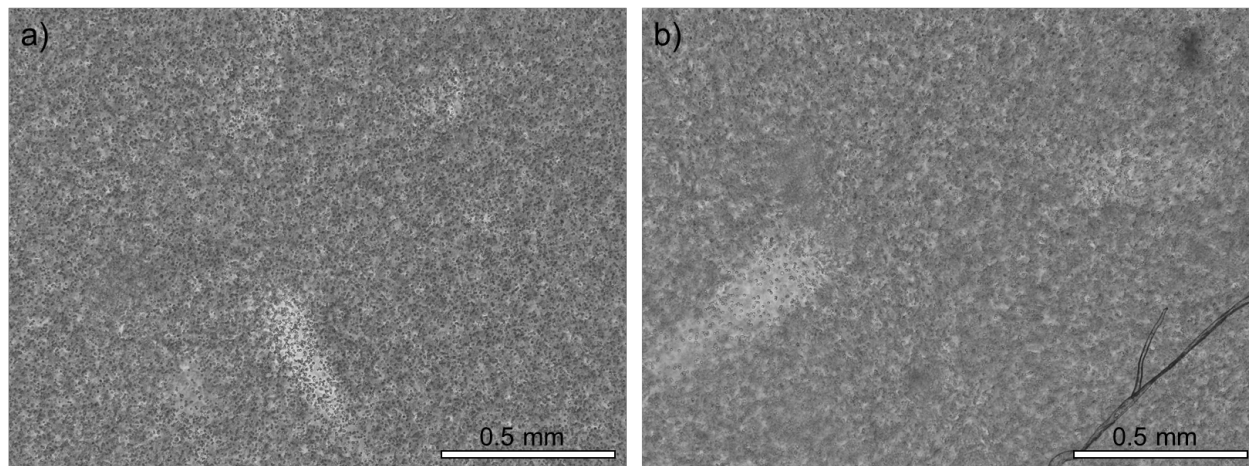


Figure S11. Optical microscope images of RBC phantoms after HIFU treatment for 30 s at a pulse duration of 16.8 μs and peak negative pressure of 16.8 MPa. a) In the absence of nanoparticles. b) In the presence of MSN ($200 \mu\text{g mL}^{-1}$).

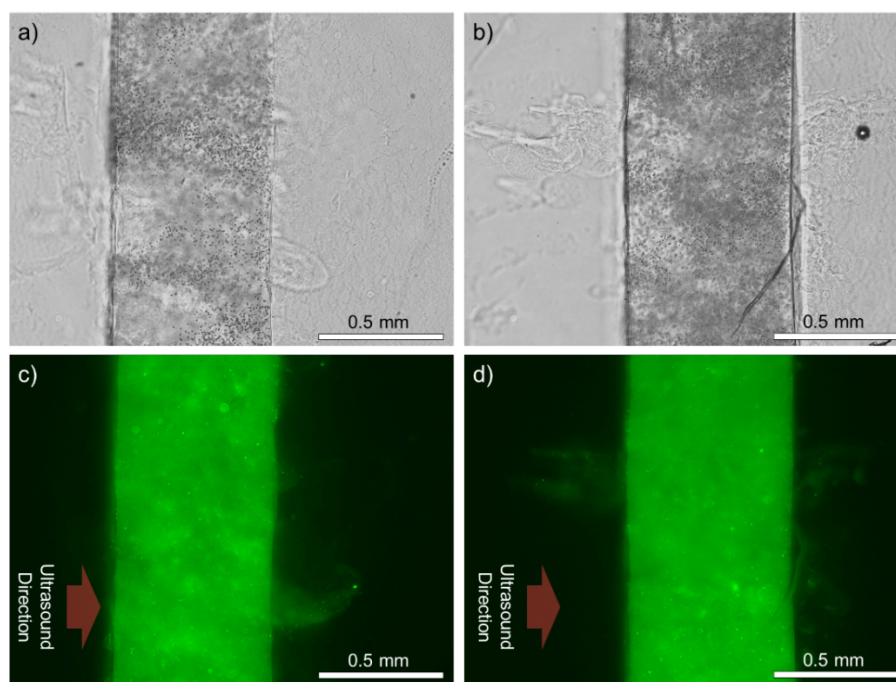


Figure S12. Additional cross-sectional bright field (a and b) and fluorescence (c and d) microscope images of the HIFU treated agarose phantoms containing PL-hMSN ($200 \mu\text{g mL}^{-1}$). Phantoms were exposed to HIFU for 30 s at a pulse duration of 16.8 μs and peak negative pressure of 16.8 MPa.

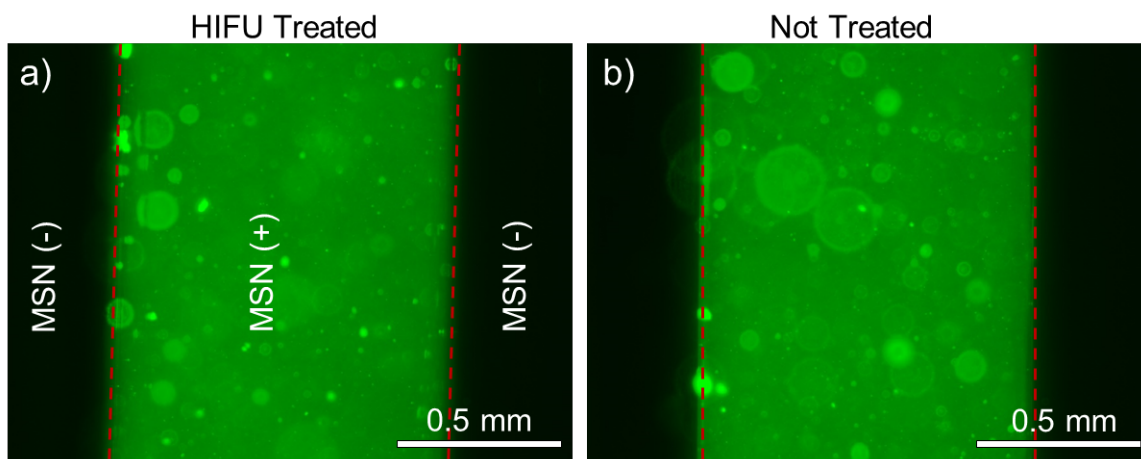


Figure S13. Cross-sectional fluorescence microscope images of the RBC phantoms containing MSN ($200 \mu\text{g mL}^{-1}$) and treated (a) or not treated (b) with HIFU for 30 s at a pulse duration of $16.8 \mu\text{s}$, a pulse repetition frequency of 10 Hz (duty cycle of 0.017%), and peak negative pressure of 16.8 MPa.

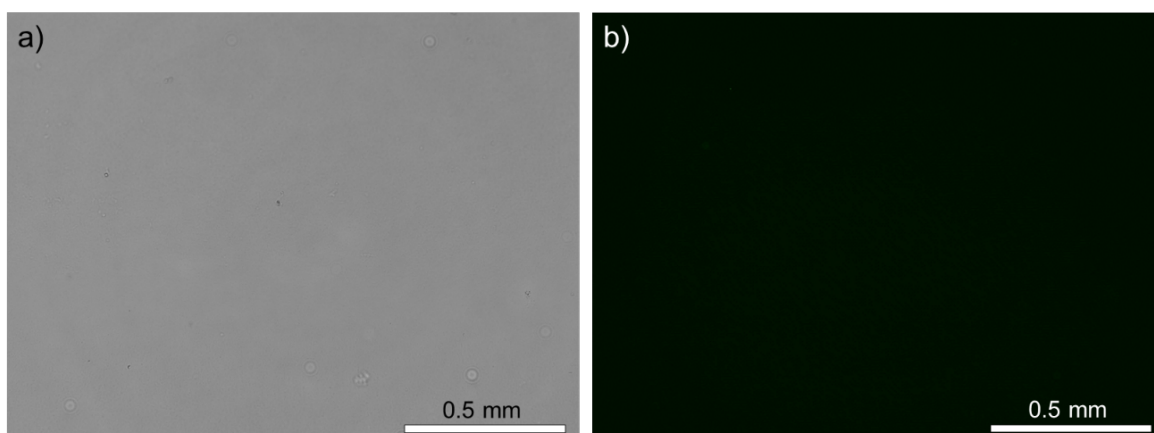


Figure S14. Bright field (a) and fluorescence (b) images of the untreated agarose gel, which was placed on top of a PL-hMSN containing agarose gels.

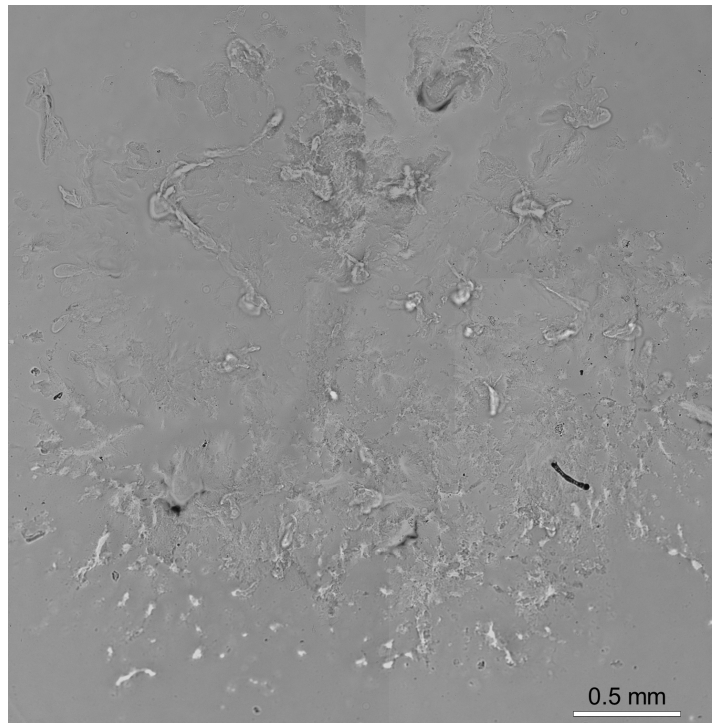


Figure S15. Bright field microscope image of the HIFU treated (for 30 s at a pulse duration of 16.8 μs , a pulse repetition frequency of 10 Hz, and peak negative pressure of 16.8 MPa.) agarose gel, which was placed on top of a PL-hMSN ($200 \mu\text{g mL}^{-1}$) containing agarose gel during HIFU treatment.

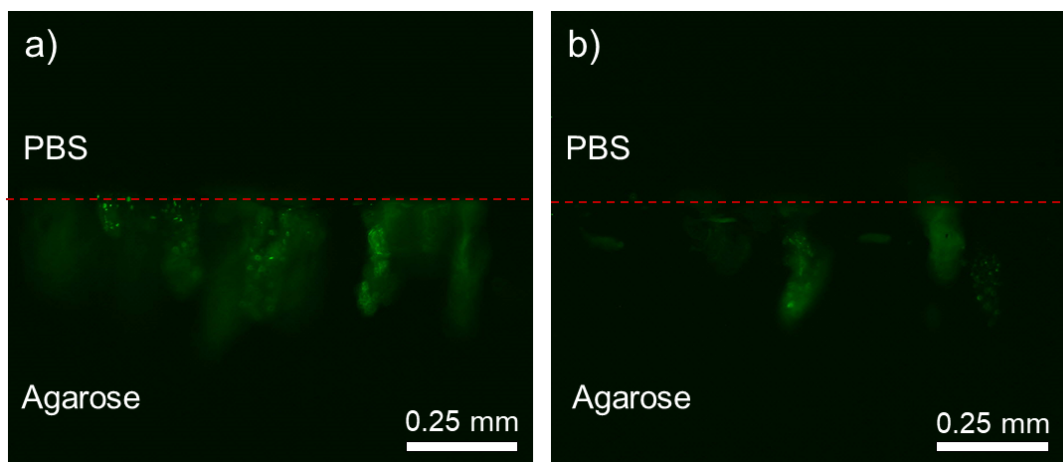


Figure S16. Additional cross-sectional fluorescence microscope images (a and b) of the HIFU treated (for 30 s at a peak negative pressure of 16.8 MPa, a pulse duration of 16.8 μs , and a pulse repetition frequency of 10 Hz) agarose gels, which were placed on top of a PL-hMSN ($200 \mu\text{g mL}^{-1}$) containing agarose gels during HIFU treatment.

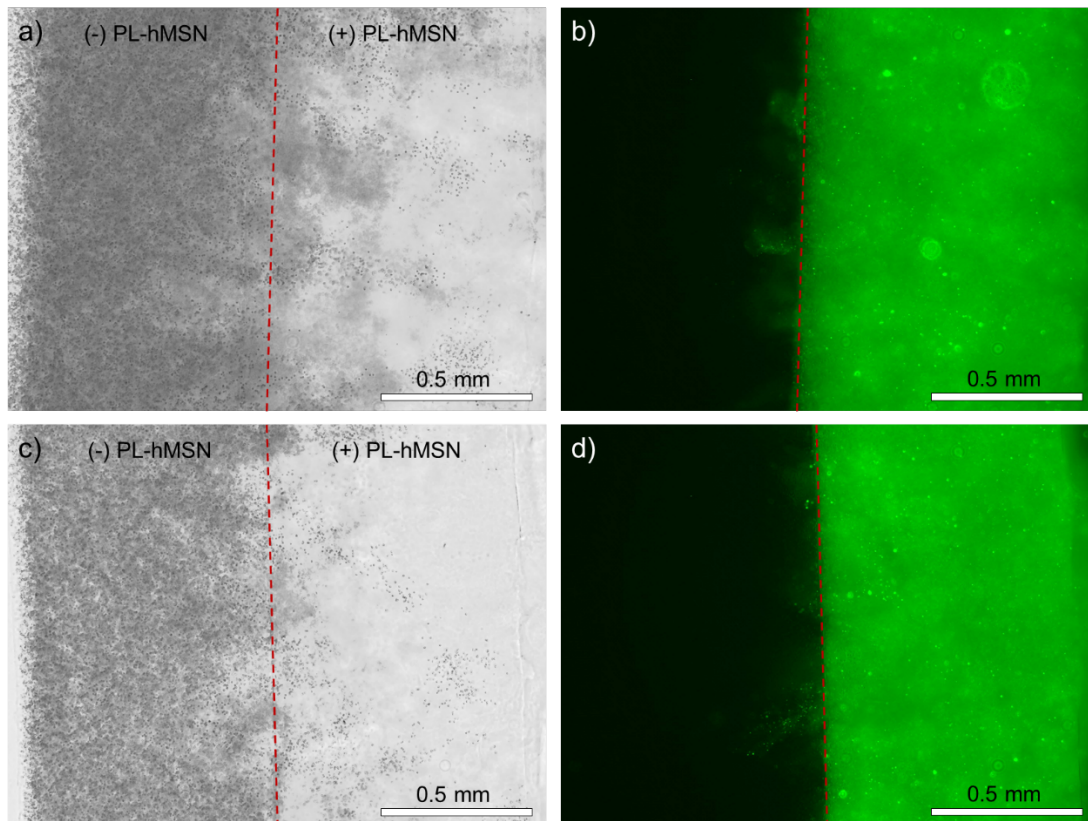


Figure S17. Additional cross-sectional bright field (a and c) and fluorescence (b and d) microscope images of the HIFU treated 4-layered agarose phantoms containing PL-hMSN ($200 \mu\text{g mL}^{-1}$) in one of the middle layers. Phantoms were exposed to HIFU for 30 s at a pulse duration of $16.8 \mu\text{s}$, a pulse repetition frequency of 10 Hz (duty cycle of 0.017%), and peak negative pressure of 16.8 MPa.

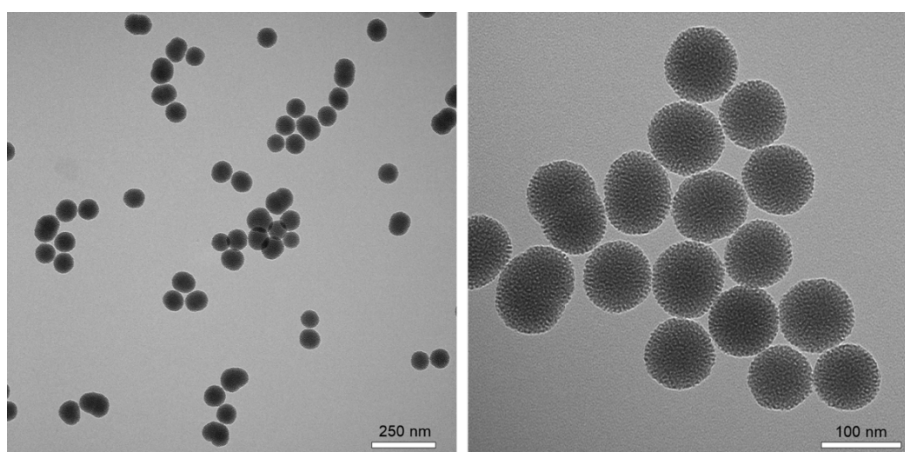


Figure S18. TEM images of the MSN prepared in the absence of fluorescein labeling for spheroid experiments.

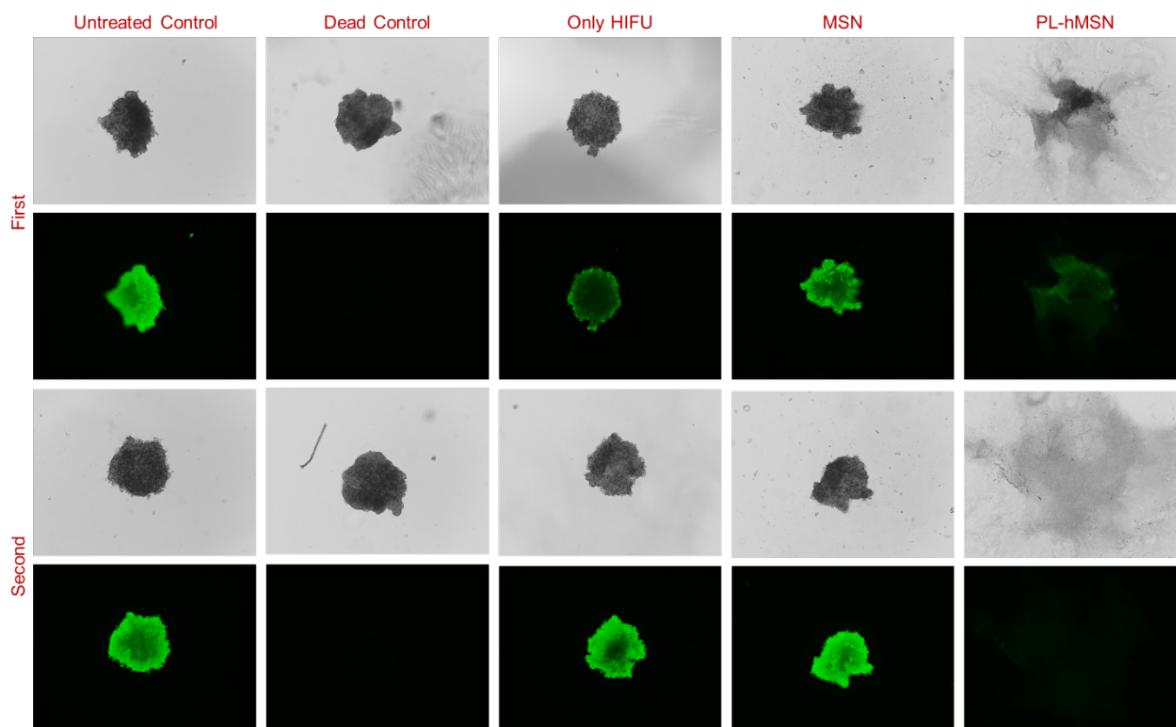


Figure S19. Additional bright field and fluorescence images of Calcein AM stained spheroids, which were treated or untreated with HIFU in the presence of ($200 \mu\text{g mL}^{-1}$) or in the absence of nanoparticles as indicated. Spheroids were exposed to HIFU for 30 s at a pulse duration of $16.8 \mu\text{s}$, a pulse repetition frequency of 10 Hz (duty cycle of 0.017%), and peak negative pressure of 16.8 MPa.

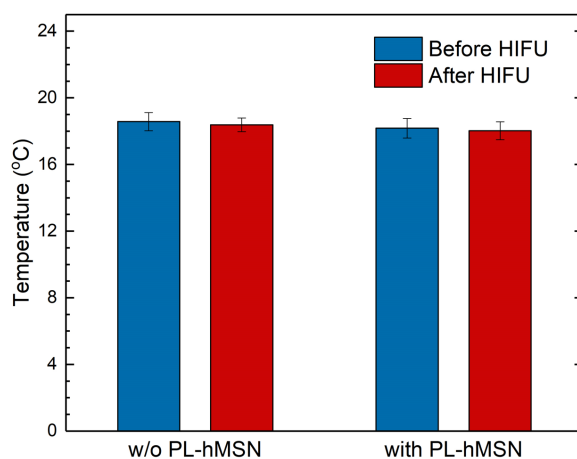


Figure S20. Temperatures of the agarose phantoms before and after HIFU treatment for 1 min at a pulse duration of $16.8 \mu\text{s}$, a pulse repetition frequency of 10 Hz (duty cycle of 0.017%), and peak negative pressure of 16.8 MPa, and in the presence or absence of PL-hMSN ($200 \mu\text{g mL}^{-1}$). Error bars = 1 SD, studies were run in triplicate.

References

1. Preston, R. C. Hydrophone-based measurements on a specific acoustic pulse. Part 1. Field characterisation. in *Output Measurements for Medical Ultrasound*; Preston, R. C., Ed.; Springer-Verlag, 1991, 93.
2. Kim, J. M.; Chang, S. M.; Kong, S. M.; Kim, K. S.; Kim, J.; Kim, W. S., Control of hydroxyl group content in silica particle synthesized by the sol-precipitation process. *Ceram. Int.* 2009, 35 (3), 1015-1019.
3. Yildirim, A.; Chattaraj, R.; Blum, N. T.; Goodwin, A. P., Understanding Acoustic Cavitation Initiation by Porous Nanoparticles: Toward Nanoscale Agents for Ultrasound Imaging and Therapy. *Chem. Mater.* 2016, 28 (16), 5962-5972.